

FIRST MEASUREMENTS WITH THE TEST STAND FOR OPTICAL BEAM TOMOGRAPHY

Christopher Wagner, Oliver Meusel, Ulrich Ratzinger, Hermine Reichau,
IAP, Frankfurt am Main, Germany

Abstract

A test stand for optical beam tomography was developed. As a new non-destructive beam-diagnostic system for high current ion beams, the test stand will be installed in the low energy beam transport section (LEBT) of the Frankfurt Neutron Source (FRANZ [1]) behind the chopper system. The test stand consists of a rotatable vacuum chamber with a mounted CCD camera. The maximum rotation angle amounts to 270° . In a first phase the optical beam profile measurement and 3D density reconstruction is tested with a time independent 10 keV He beam. The measurements and performance of data processing algorithms are compared with the beam transport simulations. In a later phase the performance with time dependent beams (120 keV, 200 mA) at a repetition rate of 250 kHz and a duty cycle of 2.5% has to be evaluated. An overview of the first phase results is shown.



Figure 1: Test stand for optical beam tomography.

INTRODUCTION

For high intensity ion beams classical destructive analysing methods become complicated. When measuring beam parameters destructively the measuring device will dissipate beam power. For the LEBT at FRANZ this means 24 kW power dissipation for a 120 keV proton beam at 200 mA. Given that this power cannot easily be dissipated by wires and similar devices non destructive methods to measure beam parameters have to be developed. With optical methods a huge set of beam parameters can be measured without beam destruction. Therefore a test stand to examine the potential of optical tomography for ion beams was developed.

TEST STAND

The designed test stand consists of a rotatable vacuum chamber mounted in a ball bearing and three viton gaskets at each end. The chamber walls are surface processed with a sandjet and blackened by an electrochemical process. This treatment is needed as the reflections within the chamber have to be minimised. The outcome of a first vacuum test for this system was a pressure of $3 \cdot 10^{-8}$ mbar. The chamber position control is performed by a magnetic angular sensor with a resolution of 3600 impulses per turn. A stepper motor connected with a drive belt system rotates the chamber. In Fig. 1 the test stand is shown. For different diagnostic instruments there are four DN100CF flanges with 90° offset connected to the rotating chamber. The camera with vacuum window is mounted at one flange and a blackened flange is mounted at the opposite side.

EXPERIMENTS

Beam Induced Fluorescence

For low energy ion beams we used the geometric cross section to calculate the photon number produced by residual gas excitation. This number can be estimated for a beam using

$$N_{\text{photon}} = \frac{\sigma}{4ek_B T} \cdot \frac{r_{\text{lens}}^2 \cdot c_{\text{corr}}}{r_{\text{dist}}^2} \cdot x \cdot p \cdot I \cdot t \quad (1)$$

with c_{corr} as the area correction factor between optical aperture and CCD area, r_{dist} as the lens distance from beam, x the observed beam length, p the residual gas pressure, I the beam current and the exposure time t . The produced photon number is linear depends linearly on beam current, residual gas pressure, exposure time and image width as shown in Eq. 1. This behavior was verified in previous experiments [4] with a 20 keV He beam and nitrogen as residual gas. A linear scaling from luminosity density to particle density will be investigated with developed tomography system in detail.

Vignetting

While taking optical beam profiles we analysed the photon count along image columns perpendicular to the beam propagation axis. As no particles should be lost during a

drift this sum has to be equal for all columns, but we noticed an intensity drop to the edges. This is caused by natural illumination falloff and could widely be corrected with the analytical function

$$I_{corrected}(\vec{r}) = I(\vec{r}) \cdot \cos^{-4} \left(\frac{|\vec{r}| \cdot \alpha}{|\vec{r}_{max}|} \right) \quad (2)$$

where the corrected intensities $I_{corrected}$ are calculated from original intensities I , the distance \vec{r} normalised to the maximum distance \vec{r}_{max} and the camera opening angle α . For more precise corrections camera falloff measurements are planned.

Camera Adjustment

During first chamber commissioning with a centered twine, we noticed an apparent twine movement between images taken at angles from 0° to 180° even though a centered object (on-axis) should not move between images. After further investigations we recognised that with our current camera mount at the vacuum window a precise position calibration is not realisable. In addition we identified the objective having too much movement tolerance causing gravity force dependent image section movement. This movement was stopped using a fixation ring connected to the camera mount. In order to correct camera misalignments the 0° and 180° images can be used since the images contain the same information but are taken from different angles. To detect a rotational and shifting misalignment the ion beam axis of both images can be compared and correction parameters estimated. A basic method is shown in Fig. 2. The beams at 0° and at 180° are plotted together with their beam axes and the estimated correction axis. For rotational misalignment correction the beam axis angle at 0° and at 180° are added to calculate the correction angle. To correct shift misalignment the distance of each beam axis to the center axis is determined and subtracted for shift

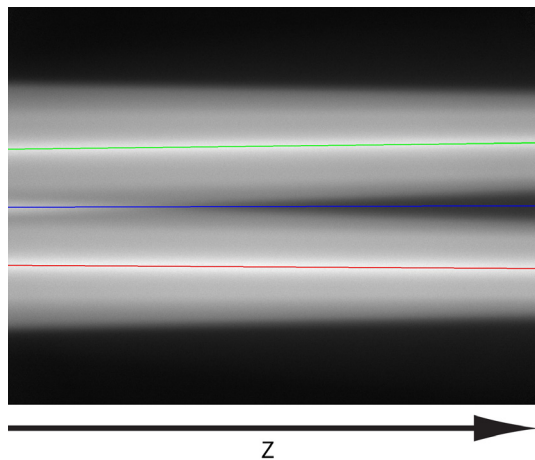


Figure 2: Estimation of correction parameters (center line, blue) by the use of fitted beam axis for beam at 0° (upper line, green) and beam at 180° (lower line, red).

correction estimation. Another correction approach reconstructs the luminosity density in the center of mass system (cms). As a major disadvantage of cms correction approach the beam position cannot be reconstructed anymore.

Tomographic Measurements

At first phase we built an elementary test environment as shown in Fig. 3. It consists of a 10 keV He ion source, a solenoid with a magnetic field up to 0.66 T, a slit-grid emittance measurement system, the rotational vacuum chamber and a faraday cup. In a first measurement the 10 keV He beam was focused with 0.21 T resulting in a beam diameter of approximately 13 mm at the image section. Nitrogen was used as residual gas at this stage. For tomographic measurements 181 beam and background images from 0° to 180° were taken. Before reconstruction backgrounds were subtracted and vignetting corrected. The tomographic reconstruction [3] as shown in Fig. 4 was calculated using the basic shift correction algorithm mentioned before.

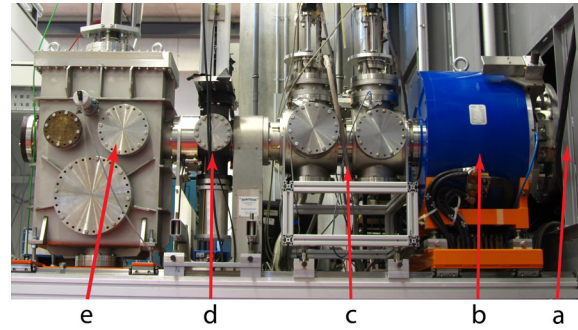


Figure 3: Test environment for first measurements: (a) 10 keV He ion source, (b) solenoid (max 0.66 T), (c) slit-grid emittance measurement system, (d) rotatable vacuum chamber with camera, (e) faraday cup.

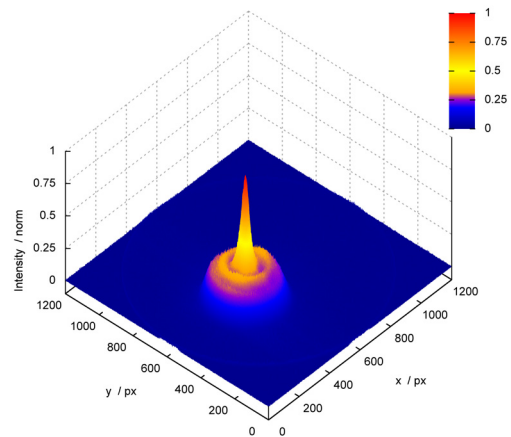


Figure 4: Luminosity density slice through beam, reconstructed via 181 measured profiles from 0° to 180° . Ring structures become visible.

As a comparison we measured the xx' plane particle distribution with the slit-grid emittance measurement system. This distribution was calculated in forward direction and optical profiles at camera position were generated using LINTRA [5]. In Fig. 5 generated profile and measured profile integrated over z are shown.

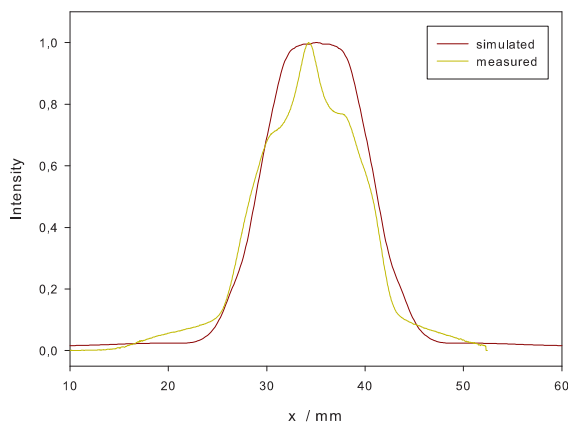


Figure 5: Beam profile taken at 0° in the rotating vacuum chamber and simulated profile integrated over z . Asymmetric drop off from maximum to beam boundaries is visible in measured profile.

CONCLUSION

A test stand for optical beam tomography was successfully developed and commissioned. Preliminary measurements of residual gas excitation and optical aberrations were done and included in the reconstruction algorithm. The first tomographic measurements with this test stand are promising. Comparison with slit-grid measurements and beam transport simulations will be done. To test system and algorithm performance we plan to use apertures to generate a well-defined beam envelope. In addition we want to use potential barriers to examine the impact of electrons on photon generation and their influence when reconstructing beam luminosity densities [2].

REFERENCES

- [1] U. Ratzinger, L.P. Chau, H. Dinter, M. Droba, M. Heilmann, N. Joshi, D. Mäder, A. Metz, O. Meusel, I. Müller, Y. Nie, D. Noll, H. Podlech, R. Reifarth, H. Reichau, A. Schempp, S. Schmidt, W. Schweizer, K. Volk, C. Wagner, C. Wiesner. *The Frankfurt Neutron Source FRANZ*. Proceedings of IPAC, MOPECO59, 2010.
- [2] F. Sittinger. *Untersuchungen zu optischen Profil- und Emittanzmessungen an niederenergetischen intensiven Ionenstrahlen*. PhD thesis, Goethe Universität Frankfurt am Main, 1995.
- [3] H. Reichau, O. Meusel, U. Ratzinger, and C. Wagner. *Estimation of profile length in hybrid ion beam tomography*. Proceedings of BIW, TUPSM059, 2010.
- [4] C. Wagner. *Entwicklung eines Teststandes für die optische Strahltomographie*. B. Sc. thesis, Goethe Universität Frankfurt am Main, 2010.
- [5] O. Meusel J. Pozimski. *LINTRA ein Computerprogramm zur Berechnung des Strahltransportes teilkompensierter, hochperveanter Ionenstrahlen*. GrakoNews (Herausgeber: Graduiertenkolleg Physik und Technik von Beschleunigern), 1/1999:33–34, 1999.